

Cite this: *Soft Matter*, 2012, **8**, 3988

www.rsc.org/softmatter

PAPER

## Particle configurations and gelation in capillary suspensions

Erin Koos\* and Norbert Willenbacher

Received 12th December 2011, Accepted 6th February 2012

DOI: 10.1039/c2sm07347a

When a small amount (less than 1%) of a second immiscible liquid is added to the continuous phase of a suspension, the rheological properties of the admixture are dramatically altered and can change from a fluid-like to a gel-like state. These so-called capillary suspensions transition to a gel-like state both if the secondary liquid preferentially wets the particles (pendular state) and even if the secondary liquid wets the particles less well than the primary fluid (capillary state). The mechanism of network formation and the distribution of the secondary liquid in the capillary state has not been investigated so far. Here, we discuss the formation of particle clusters—which are assumed to be the basic building blocks of the observed sample-spanning network—as a function of the contact angle and secondary fluid volume. The presence and strength of these clusters is directly related to the experimentally observed rheological features of capillary state suspensions.

### Introduction

Capillary suspensions, suspensions with a small amount of a second immiscible liquid, are a new class of materials with a broad spectrum of potential applications.<sup>1,2</sup> The addition of a secondary fluid can either reinforce an existing sample-spanning network created by, *e.g.*, the van der Waals force or even create a network when the particles are well stabilized.<sup>3–5</sup> Capillary suspensions can be used to suspend hydrophilic particles in hydrophobic liquids (and *vice versa*) without lavish design of particle surface properties. The phenomenon can be used to adjust the flow properties of coatings, adhesives or other complex fluids according to the requirements in particular processing steps or it may even be used to create low-fat food products with appropriate texture. The capillary force is usually much stronger and dominates over other forces.<sup>6–8</sup> Accordingly, the strong network found in these materials provides a new pathway for the creation of microporous membranes, foams and ceramics with unprecedented high porosity and small pore sizes.<sup>9</sup>

Previous investigations have shown that capillary suspensions can transition to a gel-like state at volume fractions as low as  $\phi = 0.10$ —well below the limit of dense packing—increasing the yield stress and viscosity by several orders of magnitude as the volume fraction of the second fluid is increased.<sup>1</sup>

Depending on the wetting angle of the secondary fluid, two distinct states are defined. In the pendular state, the secondary fluid preferentially wets the particles and pendular bridges form between particles. The particle–fluid admixture is in the capillary state when the secondary fluid does not preferentially wet the particles.

In the capillary state, the volume between particles is filled with the secondary liquid, as shown in the inset of Fig. 1. This schematic drawing shows two connected clusters with the secondary fluid occupying the space in the middle of each cluster. The corresponding microscopic image is shown as the main image in this figure. Here, a capillary suspension was created at a volume fraction of  $\phi = 0.3$  and further diluted in order to image the mixture. This process broke the sample-spanning network into flocs, several of which appear in this figure. In the main image, only the outline of each secondary fluid droplet is highlighted. The location of these droplets was obtained from overlaying

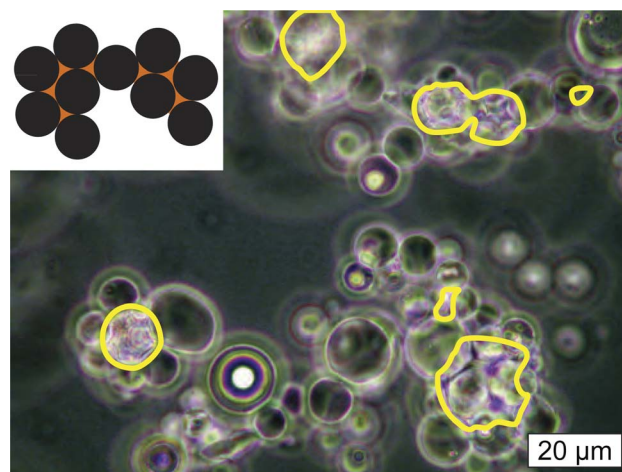


**Fig. 1** Hydrophobically modified glass beads ( $\theta = 99.3^\circ$ ,  $r = 9.6 \mu\text{m}$ ) in diisononyl phthalate with 1% wt. added water. Water droplets are outlined with a thick line (yellow/light gray). The suspension was prepared at  $\phi = 0.3$  and then diluted before imaging. *Inset*: Schematic drawing of two connected clusters of particles surrounding a secondary fluid droplet.

Institute for Mechanical Process Engineering and Mechanics, Karlsruhe Institute of Technology, Gotthard-Franz-Straße 3, Bldg. 50.31, 76131 Karlsruhe, Germany. E-mail: erin.koos@kit.edu

a fluorescent image (with edge detection) onto the white light image where a fluorescent dye (PromoFluor-488 Premium, carboxylic acid) was added to the secondary fluid. As evident in Fig. 1, larger clusters are composed of smaller particle groupings with a secondary fluid core. The size of these droplets is close to or smaller than the particle size, such that the normalized droplet volume  $V_l/r^3 \lesssim 1$ , where  $V_l$  is the droplet volume and  $r$  is the particle radius. This differs from typical Pickering emulsions where the droplet volume is typically much larger than the particle size,  $V_l/r^3 \gg 1$ .<sup>10–12</sup>

The configuration of clusters, forming the basic building blocks of a capillary suspension, will depend on the wetting angle and on the amount of secondary fluid present. Previously, small particle number clusters have been formed through the evaporation of the disperse phase of a Pickering emulsion<sup>13–17</sup> or through the use of particles with short range attractions suspended in a fluid.<sup>18,19</sup> The method for preparing these clusters strongly influences the type of clusters that are formed: the evaporation of a Pickering emulsion yields well-defined clusters of regular polyhedra with high symmetry,<sup>20</sup> whereas sticky particles form a statistical mixture of different cluster types, the majority of which have low symmetry.<sup>18</sup>

In this paper, we discuss the formation of clusters of small particle numbers surrounding a droplet of a secondary, immiscible fluid. These clusters were modeled using the computational code Surface Evolver as a function of the number of particles, volume of the droplet, and the wetting angle between the solid and secondary fluid. Limits on the formation of these clusters and their strength correspond to experimentally determined yield stress and shear modulus data for capillary suspensions.

## Experimental methods

The capillary suspensions are characterized using the saturation of the preferentially wetting fluid  $S$ ,

$$S = \frac{\nabla_{\text{wetting fluid}}}{\nabla_{\text{total fluid}}} = \frac{\nabla_b}{\nabla_b + \nabla_l}, \quad (1)$$

which is close to zero for the pendular state and approaches one for the capillary state.<sup>21,22</sup> Here, the symbol  $\nabla_l$  represents the total secondary fluid volume in a sample as opposed to  $V_l$  which represents the secondary fluid droplet volume in an individual particle cluster. The total volume of the bulk fluid is given by  $\nabla_b$ . Capillary suspensions are also characterized by the two-fluid wetting angle as measured into the secondary fluid, such that in the capillary state  $\theta > 90^\circ$ .

## Computational model

The computational code Surface Evolver, designed by Brakke<sup>20,23</sup> was used to model the formation of capillary state clusters. This method seeks to minimize the energy of a fluid surface subject to the chosen constraints (*e.g.* secondary fluid droplet volume and contact angle). In this case, the secondary fluid was confined to the inner region of a stationary close-packed cluster of particles and the bulk fluid was not modeled. To preserve the contact angle at the particle–fluid interface, the surface energy must satisfy the Young equation,

$$\Gamma_{sb} - \Gamma_{sl} = \Gamma_{bl} \cos\theta, \quad (2)$$

where the subscript  $s$  represents the solid surface,  $b$  the bulk fluid and  $l$  the secondary liquid.<sup>24</sup> The surface energy per unit area is given by  $\Gamma_{\alpha\beta}$  and the wetting angle of the secondary fluid by  $\theta$ .

For each cluster configuration, both the contact angle and volume of the secondary fluid droplet were changed. The droplet volume was always normalized by the particle radius, such that  $\tilde{V}_l = V_l/r^3$ . The Surface Evolver model, starting with coarse polyhedral areas, iteratively moved the interfaces to minimize the energy.<sup>23</sup> The interfaces were refined and iteratively minimized several times until further iterations or refinement did not influence the resulting energy. Two example clusters, both with 5 particles arranged in a triangular bipyramid, are shown in Fig. 2. The secondary fluid in both clusters have the same contact angle and total droplet volumes.

Nine different particle configurations were studied representing all possible close-packed structures using between 4 and 7 particles. The  $n = 6$  and  $n = 7$  structures, where  $n$  is the number of particles in each cluster, include new seed groupings ( $n = 6$  octahedral and  $n = 7$  pentagonal bipyramid) as well as structures composed of smaller seeds (*i.e.* polytetrahedral structures).<sup>25</sup> The structures composed of two or more seeds were modeled using both contiguous as well as two or more isolated secondary fluid droplets within one cluster (as shown in Fig. 2). Each contiguous droplet was modeled individually, but the energy landscape of separated droplets was calculated from the corresponding seed clusters (*e.g.* two tetrahedrons for the triangular bipyramid). The minimum energy for a single cluster with separated droplets was found by considering the energy of seed clusters with differing droplet volumes, which together equaled the total droplet volume to be determined, and finding the minimum of all of the possible configurations. Once the energy and stability ranges for all of the cluster configurations were computed, the final minimum energy diagram was calculated. Transition lines between minimum energy configurations were calculated as the point where the reduction in energy for these two clusters were equivalent.

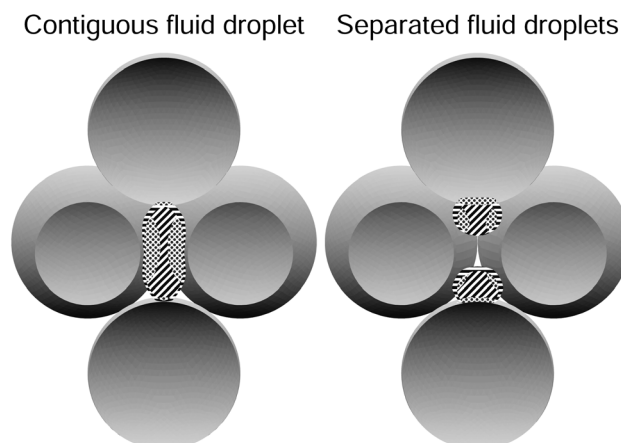


**Fig. 2** Cutaway images of two example clusters of 5 particles arranged in a triangular bipyramid shown with a contiguous fluid droplet and two separated fluid droplets. Stripes represent interfaces with the bulk fluid and dots represent interfaces with the solid particles. The total normalized droplet volume  $\tilde{V}_l = 0.2$  and the contact angle  $\theta = 120^\circ$ .

## Sample preparation

Experiments were conducted using two different particle systems: glass and calcium carbonate. The calcium carbonate particles were manufactured by Solvay Advanced Functional Minerals (Socal U1S1, Salin de Giraud, France) with an average diameter of 1.6  $\mu\text{m}$ . The glass, obtained from Potters Europe (Spherglass 3000 and 5000 Solid Glass Microspheres, Kirchheimbolanden, Germany), was sieved to create the desired particle size distribution with a diameter of 9.6  $\mu\text{m}$ . The particle sizes, were measured using using LALLS (Low Angle Laser Light Scattering, Sympatec HELOS H0309) when suspended in ethanol and subjected to ultrasonic dispersion. (The particles were suspended using a Sympatec QUIXEL unit.) The calcium carbonate particles were hydrophobically modified by the manufacturer and were not treated further. The glass was treated with 98% trimethylsilyl chloride (TMCS) as provided by Alfa Aesar to achieve the desired contact angles.<sup>26–28</sup>

The samples used throughout this paper were created using thoroughly dried particles (dried overnight at 70 °C), which were suspended in either silicone oil (AK200, Wacker Chemie AG, Burghausen, Germany) or diisononyl phthalate (DINP, Henkel AG, Düsseldorf, Germany) with added water. The particles were mixed into the bulk fluid using a turbulent beater blade until a uniform suspension was created (at 500–2000 rpm for 20 min). This mixture was again dried overnight at 70 °C to remove any water that may have condensed during mixing and held under vacuum (100 mbar) to remove air bubbles. At room temperature, the secondary fluid was added to the suspension and thoroughly mixed using a propeller stirrer (at 500–1000 rpm for 10 min). The samples were held in airtight containers until the measurements were completed.

The mixtures are also characterized by the two-fluid wetting angles, which are calculated from the wetting angles that the individual fluids make with respect to the particles in air. The fluid wetting angles were determined using a modified Washburn method for the capillary rise of a fluid through a dry powder in air<sup>29</sup> using a DataPhysics DCAT 21 tensiometer (Filderstadt, Germany). For fluid–particle combinations with contact angles greater than 90° in air, *i.e.*, hydrophobic particles in water, particles were attached to a Wilhelmy plate using double-sided tape and the advancing contact angle was measured.<sup>30</sup> These values were adjusted to account for errors due to surface roughness following the method of Yan.<sup>31–33</sup> Using the values determined in air, the two-liquid wetting angle is calculated using the Young equation<sup>10,34</sup> as

$$\cos \theta_{l,b} = \frac{\Gamma_{la} \cos \theta_{l,a} - \Gamma_{ba} \cos \theta_{b,a}}{\Gamma_{bl}}, \quad (3)$$

where the subscript *a* refers to air, *b* the primary (bulk) liquid, and *l* the secondary liquid. The wetting angle  $\theta_{\alpha,\beta}$  is the angle fluid  $\alpha$  makes against the solid in an environment provided by fluid  $\beta$ . The interfacial tension  $\Gamma_{\alpha\beta}$  is measured at an interface between the two fluids, as was measured using a Wilhelmy plate on the same tensiometer.

## Rheological data

The strength of capillary suspensions is primarily measured through the yield stress. These measurements were conducted

using a cone–plate rheometer (RheoScope 1, Thermo Fisher Scientific, Karlsruhe, Germany). The yield stress is defined as the stress at which the mixture begins to flow, that is, to deform plastically. These measurements were conducted using a stress-ramp where the yield stress was found as the point at which slope of the logarithmic deformation (as a function of the logarithmic shear stress) changes from a very low (nonzero) value to a high value. Further confirmation of yield was provided by a drastic reduction in the measured viscosity. These points were evaluated using the RheoWin software and a Matlab algorithm. For most samples, the shear stress ramp was conducted between 10 Pa and 1000 Pa with 1000 sample points over 20 min. Samples with lower or higher yield stress required lower or higher ramp limits, spanning at least two orders of magnitude (beginning at least one order of magnitude below the expected yield stress value). Experiments were repeated several times to ensure that the ramp limits were sufficient and that the experimental values were consistent.

Small amplitude oscillatory shear measurements were conducted in the linear viscoelastic regime to identify the complex shear modulus  $G^*$ . This linear viscoelastic regime was identified using a stress amplitude ramp at the desired frequency (or range of frequencies). Actual measurements of the shear modulus were conducted in this linear regime, well below the yield stress, using a stress controlled rheometer (MARS, Thermo Fisher Scientific, Karlsruhe, Germany) in a cone–plate configuration.

## Results and discussion

### Computational results

The computational model yielded several preliminary results that were used to understand the energy landscape for cluster formation. For every case where a cluster could have either a contiguous fluid droplet or two or more separated droplets, the separated droplets always resulted in a lower energy state. Usually, the lowest energy state for these separated droplets occurs when the individual droplet volumes are all the same size for polytetrahedral clusters.

To confirm the assumption of a close-packed particle structure, both  $n = 4$  tetrahedral and  $n = 5$  triangular bipyramid structures were modeled where the particles were not fixed. The surface energy between the particles and bulk fluid was set as ten times the surface energy between the two fluids ( $\Gamma_{sb} = 10\Gamma_{sl}$ ) such that the particles retained a spherical shape (as has been done for clusters formed from Pickering emulsions<sup>20,35</sup>). The positions of the particles were tracked for various droplet volumes and contact angles and compared to the close-packed positions. At high droplet volumes, the moveable particles were displaced from the close-packed structure (such that there was a gap between adjacent particles). The volume required to move the particles occurred at volumes higher than the transition lines to a higher particle number cluster and would not influence the state diagram.

These preliminary results were integrated into the computational model to produce a state diagram of the lowest energy states as a function of  $\tilde{V}_l$ , the normalized secondary fluid droplet volume. This energy state diagram is shown in Fig. 3. The

maximum contact angle for the formation of stable tetrahedral (and polytetrahedral) structures is  $\theta_{c, \text{tet}} = 151.2^\circ$ . Octahedral structures are unstable for  $\theta_{c, \text{oct}} > 165.3^\circ$ . Larger secondary fluid droplets tend to form stable structures using greater numbers of particles and structures using larger seeds.

The shielding of the secondary fluid by the particles serves as an attractive capillary force between particles due to the corresponding reduction in energy. This reduction in energy is shown as the shading in Fig. 3 with all of the stable structures formed from smaller seeds having subdivided fluid droplets. This means that all  $n = 7$  polytetrahedral structures have the same  $\Delta E$  at a constant wetting angle and secondary droplet volume.<sup>36</sup> The formation of these structures, however, is not equally likely due to the differences in entropy.<sup>18</sup> The lower symmetry  $C_2$  structure is preferred over the higher symmetry  $C_{3v}$ . These anisotropic, lower symmetry clusters are better suited to create sample-spanning networks than the clusters of higher symmetry.<sup>37,38</sup> We assume, that when a capillary suspension is prepared, the secondary fluid is fragmented into small  $\mu\text{m}$ -sized droplets serving as seeds for the formation of the individual clusters discussed above, then a sample-spanning fractal network is formed due to the convection driven collisions of the basic building blocks.

### Comparison with rheological data

Previously reported experiments of capillary state suspensions show that the normalized yield stress and viscosity have a typical dependence on the wetting liquid fraction  $S$  that is independent of the volume fraction of particles.<sup>1</sup> One such curve, in this case for hydrophobically modified calcium carbonate suspended in silicone oil with small amounts of added water is reproduced in Fig. 4. For this mixture, a volume fraction of solids of  $\phi = 0.112$  was used. The dramatic rise of a yield stress in this mixture

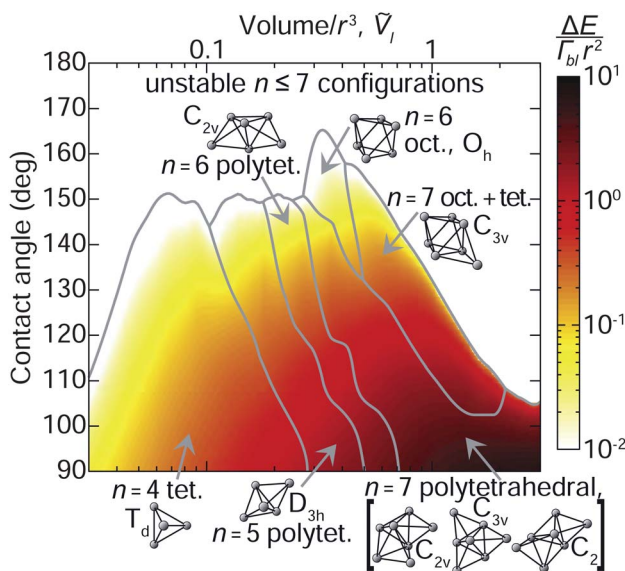


**Fig. 3** State diagram showing the minimum energy regions for various particle clusters as a function of the normalized secondary fluid droplet volume and the wetting angle  $\theta$ . Color indicates the reduction in energy compared to detached fluid drops.

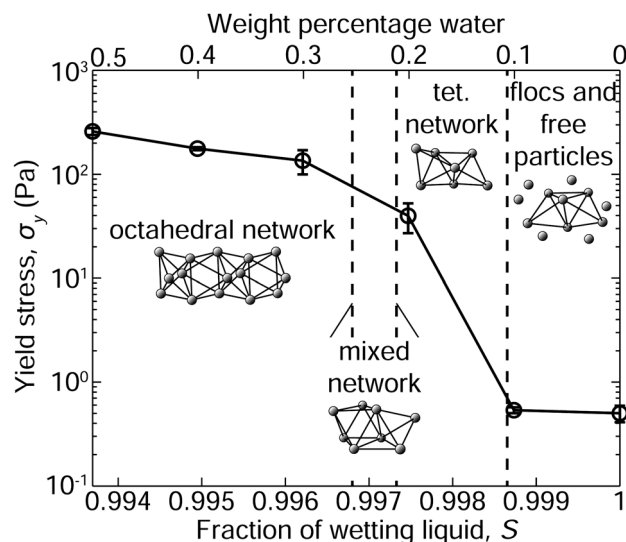


**Fig. 4** Yield stress for a  $\phi = 0.112$  suspension of  $\text{CaCO}_3$  in silicone oil with added water with  $\theta = 139.2^\circ$ . The addition of the water is shown both as a direct weight percentage and as the fraction of the liquid volume  $S$ . The dashed lines represent the transitions between regions with differing particle configurations.

implies that we must have structures of particles that span a large sample volume. There is a small yield stress present in the suspensions without added liquid due to the weak van der Waals attraction between the calcium carbonate particles. This weak attraction is quickly overtaken by the strong capillary attraction.

For networks formed by small amounts of added secondary liquid, the computational models allow us to predict the total secondary fluid volume required to produce various structure types. Using the definition of the volume fraction  $\phi = \mathbb{V}_s / (\mathbb{V}_s + \mathbb{V}_b + \mathbb{V}_l)$  and fraction of wetting liquid  $S = \mathbb{V}_l / (\mathbb{V}_b + \mathbb{V}_l)$ ,

$$S = 1 - \tilde{V}_l \frac{3}{4\pi} \frac{m}{n} \frac{\phi}{1 - \phi}, \quad (4)$$

where  $n$  particles are connected using  $m$  secondary fluid droplets. Networks of tetrahedral subgroups, with disconnected secondary fluid droplets, and octahedral groupings require

$$\begin{aligned} n_{\text{tet}} &= 3 + m_{\text{tet}}, \\ n_{\text{oct}} &= 3 + 3m_{\text{oct}}, \end{aligned} \quad (5)$$

droplets, respectively. Combining eqn (4) and eqn (5) while assuming large numbers of particles yields an equation for the fraction of wetting liquid,

$$\begin{aligned} S_{\text{tet}} &= 1 - \tilde{V}_{l,\text{tet}} \frac{3}{4\pi} \frac{\phi}{1 - \phi}, \\ S_{\text{oct}} &= 1 - \tilde{V}_{l,\text{oct}} \frac{1}{4\pi} \frac{\phi}{1 - \phi}. \end{aligned} \quad (6)$$

If we consider a volume fraction  $\phi = 0.112$  (with a contact angle of  $139.2^\circ$ , the conditions of the suspension reported in Fig. 4), we can calculate the total fraction of wetting liquid required to form different types of networks. The first formation of tetrahedral networks occurs at  $\tilde{V}_{l,\text{tet}} = 0.0461$  ( $S_{\text{tet}} = 0.9986$ , 0.11% wt. water). Below this droplet volume, there is not enough

secondary fluid to create a complete polytetrahedral network. The tetrahedral networks near this transition are quite weak and do not result in a significant increase in the yield stress, but as shown in previous work,<sup>1</sup> there is a variation in the shear modulus corresponding to a weakly percolated network. At  $\tilde{V}_{b,tet} = 0.0914$  ( $S_{tet} = 0.9972$ , 0.21% wt. water), the reduction of energy of the tetrahedral cluster is the greatest. There is a sharp rise in the measured yield stress that corresponds well to the increase in the strength of the tetrahedral cluster as the interstitial volume fills (shown by the shading in Fig. 3). Above this point, octahedral structures have a lower energy than tetrahedral structures and the network will begin to transition to an octahedral network. This transition proceeds until  $\tilde{V}_{b,oct} = 0.32$  ( $S_{oct} = 0.9968$ , 0.25% wt. water) when the network is composed completely of octahedral subgroups. These transitions are denoted in Fig. 4 using dashed lines. The octahedral network will persist until  $\tilde{V}_{b,oct} = 0.6787$  ( $S_{oct} = 0.9932$ , 0.52% wt. water) when a transition to higher order seed (and/or non-close-packed) structure will proceed.

In order to probe the relative strength of these particle networks, the network was destroyed during a period of high shear and then the shear modulus was measured as the network reformed and aged, as shown in Fig. 5. The sample was aged either under static conditions (wherein it was not subjected to any deformation until the specified time) or dynamic conditions (stress controlled oscillation at 1 Hz with  $\sim 1\%$  strain). The strong networks formed by admixtures with greater than 0.20% wt. water do not show any increase in network strength for longer static recovery times and only a weak power-law dependence for the dynamic measurements ( $G' = 5800 t^{0.16}$ ,  $G'' = 3100 t^{-0.07}$ ). The weak network formed by the mixture with 0.10% wt. water increases in strength for both  $G'$  and  $G''$  ( $G' = 0.47 t^{0.79}$ ,  $G'' = 5.6 t^{0.39}$ ). Additionally, after a short period of dynamic recovery, the modulus is much greater than under static recovery,

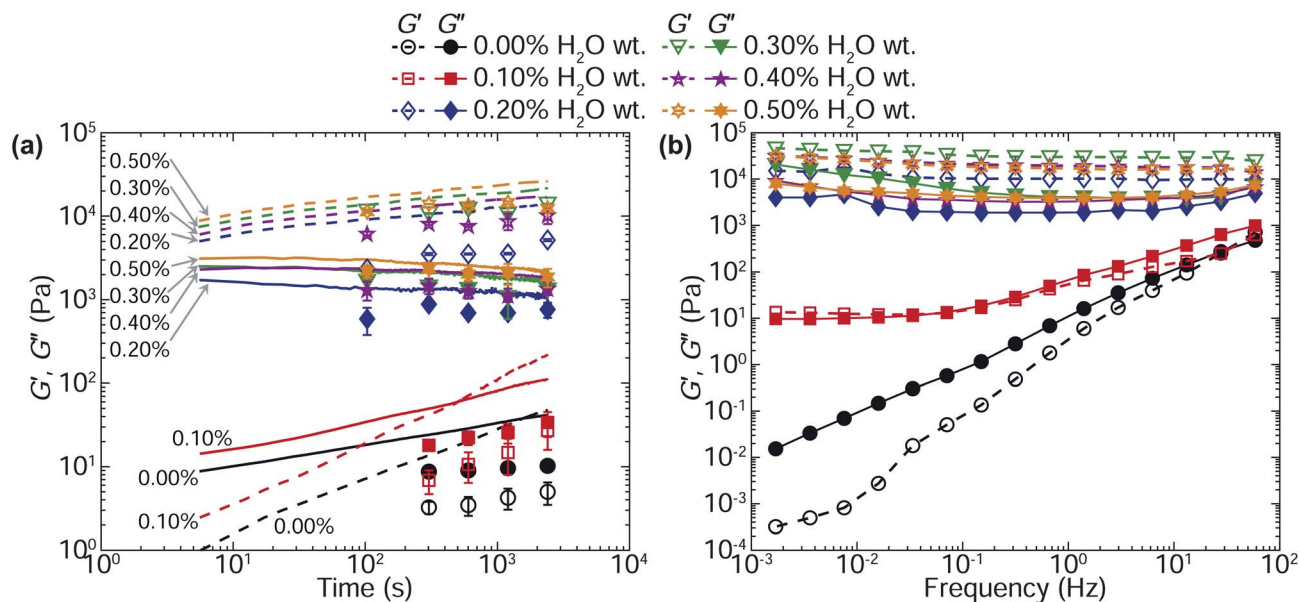


**Fig. 5** (a) Static (symbols) and dynamic (lines, dashed  $G'$  and solid  $G''$ ) network reformation for  $\text{CaCO}_3$  admixtures following a period of high shear ( $1000 \text{ s}^{-1}$ , 300 s). (b) Linear viscoelastic moduli for the same mixtures and as a function of the oscillation frequency without any preshear protocol. The network strength was measured at a strain of  $\sim 1\%$  in both tests and at a frequency of 1 Hz for the network reformation test.

indicating that under this light oscillation, the initially weak network is able to rearrange into a much stronger state.<sup>39,40</sup> The computational model for this particular admixture predicted a weak tetrahedral structure. Correspondingly, the thixotropic behavior confirms the existence of a weak network that easily reorganizes in order to increase the network strength.

The Surface Evolver model predicts that tetrahedral clusters will not be stable above the critical contact angle of  $151.2^\circ$ . Yield stress data for suspensions of glass beads with two different contact angles ( $\theta = 99.3^\circ$  and  $\theta = 159.9^\circ$ ), suspended in diisononyl phthalate ( $\phi = 0.40$ ), are shown in Fig. 6. The suspension with the smaller contact angle shows a strong increase in the yield

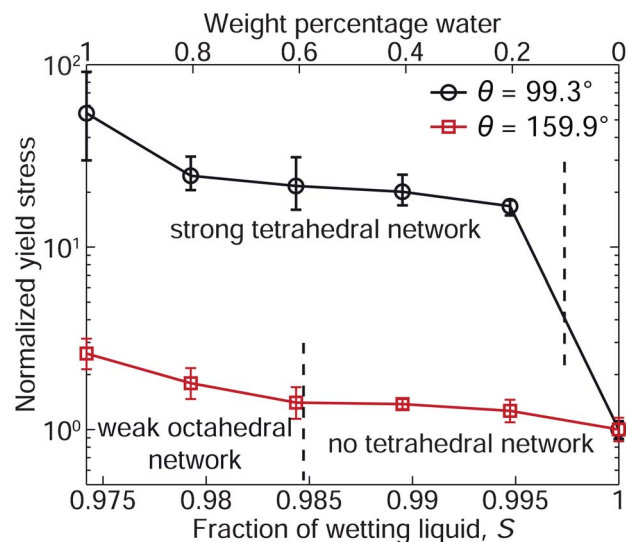


**Fig. 6** Yield stress, normalized against the measurement with no secondary liquid, for hydrophobically modified glass in diisononyl phthalate ( $r = 4.8 \mu\text{m}$ ,  $\phi = 0.40$ ) with two different contact angles.

stress with added water corresponding to the creation of a tetrahedral network ( $\tilde{V}_{l,tet} = 0.0165$ ,  $S_{tet} = 0.9974$ , 0.10% wt. water). There is almost no change in the yield stress for the more hydrophobic particles, as stable tetrahedral networks cannot be created. At this contact angle, a stable octahedral network will be formed at  $\tilde{V}_{l,oct} = 0.2880$  ( $S_{oct} = 0.9847$ , 0.59% wt. water) and is visible as the slight increase in the leftmost points. The rather modest increase in the yield stress is due in part to the only slight reduction in energy between the clustered and unclustered state at the higher contact angle. The energy reduction of the octahedral cluster at the higher contact angle (159.9°) is only 3% of the energy reduction in the tetrahedral subgrouping at the same  $\tilde{V}_l$  and lower contact angle (99.3°).

## Conclusions

The aggregation of particles around small droplets of secondary liquid represents a lower energetic state than for separated particles and secondary liquid droplets. This energetic saving may be viewed as a short-range attraction leading to the formation of particle clusters as discussed above. The transition from a fluid-like state to a highly elastic gel-like state is a result of the aggregation of these clusters into a sample-spanning network when a sufficient amount of secondary fluid is added. The formation of capillary suspensions relies on three steps: well distributed droplets of secondary fluid are created through high-shear mixing; these droplets quickly become surrounded by solid particles forming structures of small particle numbers (seed groupings); and finally, these structures merge to form large particle number networks. These steps likely occur nearly simultaneously during the mixing process. It is important to note that the shielding of small droplets by particles is not a global energy minimum—this energy state is higher than complete phase separation—but represents a metastable state; once the small droplets become surrounded by particles this subgrouping is kinetically trapped because the particle-clusters are immobilized in the network structure.

As the contact angle increases, greater amounts of secondary fluid are required to form stable clusters and their cohesive strength becomes weaker (as well as that of the corresponding network). Above a critical contact angle (e.g. 151.2° for the tetrahedral and 165.3° for the octahedral structures), particle clusters are not energetically favorable and high contact angles may explain why some particle–fluid combinations do not make strong capillary suspensions.

Capillary forces are able to form or strengthen existing sample spanning networks in various particle–fluid combinations. While there are other attractive interactions leading to gelation in colloidal suspensions, the strength of the capillary force makes these mixtures particularly interesting. While the high water content admixtures increase in strength when subjected to small amplitude oscillations, these mixtures gel very quickly following periods of high shear.

Capillary suspensions, suspensions formed through the addition of a secondary fluid, represent a new class of materials. Capillary forces can be used to vary rheological features of different classes of complex fluids in a wide range to meet the specific needs of a particular processing step or application techniques. Moreover, strong particle networks may be created,

which can be used as precursors for the manufacture of porous solids or membranes. Even if the secondary fluid does not preferentially wet the particles, a transition from a fluid-like to gel-like state is observed at secondary liquid fractions as low as 0.2% wt., suggesting the formation of a sample-spanning network of structures within the admixture. Here, we assume that small particle number clusters incorporating small liquid droplets serve as building blocks for network formation. The structure and strength of these clusters is predicted as a function of the contact angle and secondary fluid droplet volume. The rheological features of capillary state suspensions reported here can be nicely rationalized on the basis of this cluster model.

## Acknowledgements

We thank H. J. Butt and S. Herminghaus for stimulating discussions as well as the German Research Foundation (Deutsche Forschungsgemeinschaft grant no. WI3138/6-1) for funding.

## Notes and references

- 1 E. Koos and N. Willenbacher, *Science*, 2011, **331**, 897–900.
- 2 E. Koos, J. Dittmann and N. Willenbacher, *Chem. Ing. Tech.*, 2011, **83**, 1305–1309.
- 3 S. V. Kao, L. E. Nielsen and C. T. Hill, *J. Colloid Interface Sci.*, 1975, **53**, 367–373.
- 4 C. Gögelein, M. Brinkmann, M. Schröter and S. Herminghaus, *Langmuir*, 2010, **26**, 17184–17189.
- 5 K. Cavalier and F. Larché, *Colloids Surf., A*, 2002, **197**, 173–181.
- 6 H. J. Butt and M. Kappl, *Adv. Colloid Interface Sci.*, 2009, **146**, 48–60.
- 7 P. A. Kralchevsky and N. D. Denkov, *Curr. Opin. Colloid Interface Sci.*, 2001, **6**, 384–401.
- 8 *Colloid stability: The role of surface forces, Part 1*, ed. T. F. Tardos, Wiley-VCH, 2006, vol. 1.
- 9 J. Dittmann, E. Koos, N. Willenbacher and B. Hochstein, *Verfahren zur Herstellung einer porösen Keramik und damit erhältliche poröse Keramik*, German Patent DE 10 2011 106 834.5, 2011.
- 10 R. Aveyard, B. P. Binks and J. H. Clint, *Adv. Colloid Interface Sci.*, 2003, **100–102**, 503–546.
- 11 M. E. Cates, *J. Phys.: Condens. Matter*, 2005, **17**, 2771–2778.
- 12 I. Akartuna, A. R. Studart, E. Tervoort, U. T. Gonzenbach and L. J. Gauckler, *Langmuir*, 2008, **24**, 7161–7168.
- 13 V. N. Manoharan, M. T. Elsesser and D. J. Pine, *Science*, 2003, **301**, 483–487.
- 14 C. S. Wagner, Y. Lu and A. Wittemann, *Langmuir*, 2008, **24**, 12126–12128.
- 15 C. S. Wagner, B. Fischer, M. May and A. Wittemann, *Colloid Polym. Sci.*, 2010, **288**, 487–498.
- 16 A. D. Dinsmore, M. F. Hsu, M. G. Nikolaidis, M. Marquez, A. R. Bausch and D. A. Weitz, *Science*, 2002, **298**, 1006–1009.
- 17 V. N. Manoharan, *Solid State Commun.*, 2006, **139**, 557–561.
- 18 G. Meng, N. Arkus, M. P. Brenner and V. N. Manoharan, *Science*, 2010, **327**, 560–563.
- 19 N. Arkus, V. N. Manoharan and M. P. Brenner, *Phys. Rev. Lett.*, 2009, **103**, 118303.
- 20 E. Lauga and M. P. Brenner, *Phys. Rev. Lett.*, 2004, **93**, 238301.
- 21 H. Rumpf, *Agglomeration*, Interscience, John Wiley & Sons, New York, 1962, pp. 379–418.
- 22 H. Schubert, *Kapillarität in porösen Feststoffsystemen*, Springer-Verlag, Berlin, 1982.
- 23 K. A. Brakke, *Experimental Math*, 1992, **1**, 141–165.
- 24 B. P. Binks and J. H. Clint, *Langmuir*, 2002, **18**, 1270–1273.
- 25 N. Arkus, PhD thesis, Harvard University, Cambridge, MA, USA, 2009.
- 26 M. Fuji, H. Fujimori, T. Takei, T. Watanabe and M. Chikazawa, *J. Phys. Chem. B*, 1998, **102**, 10498–10504.

- 
- 27 T. Takei, A. Yamazaki, T. Watanabe and M. Chikazawa, *J. Colloid Interface Sci.*, 1997, **188**, 409–414.
- 28 L. Forny, I. Pezron, K. Saleh, P. Guigon and L. Komunjer, *Colloids Surf., A*, 2005, **270–271**, 263–269.
- 29 G. Gillies, K. Büscher, M. Preuss, M. Kappl, H. J. Butt and K. Graf, *J. Phys.: Condens. Matter*, 2005, **17**, 445–464.
- 30 S. Stiller, H. Gers-Barlag, M. Lergenmueller, F. Pflücker, J. Schulzb, K. P. Wittern and R. Daniels, *Colloids Surf., A*, 2004, **232**, 261–267.
- 31 L. Yan, K. Wang, J. Wu and L. Ye, *Colloids Surf., A*, 2007, **296**, 123–131.
- 32 R. N. Wenzel, *Ind. Eng. Chem.*, 1936, **28**, 988–994.
- 33 H. Nakae, R. Inui, Y. Hirata and H. Saito, *Acta Mater.*, 1998, **46**, 2313–2318.
- 34 C. O. Fournier, L. Fradette and P. A. Tanguy, *Chem. Eng. Res. Des.*, 2009, **87**, 499–506.
- 35 Y.-S. Cho, G.-R. Yi, J.-M. Lim, S.-H. Kim, V. N. Manoharan, D. J. Pine and S.-M. Yang, *J. Am. Chem. Soc.*, 2005, **127**, 15968–15975.
- 36 Due to the small differences in particle-bulk fluid surface area between clustered and unclustered particles and small contribution of this term, it is neglected when calculating the unclustered energy.
- 37 S. Mossa, F. Sciortino, P. Tartaglia and E. Zaccarelli, *Langmuir*, 2004, **20**, 10756–10763.
- 38 E. Zaccarelli, *J. Phys.: Condens. Matter*, 2007, **19**, 323101.
- 39 N. Willenbacher, *J. Colloid Interface Sci.*, 1996, **182**, 501–510.
- 40 A. S. Negi and C. O. Osuji, *Physical Review E*, 2009, **80**, 010404.